

# Flexural Behavior of RC Beams Strengthened with FRP Bars by Near-Surface Mounted Method

Trung Tran Le Hoang

Graduate school of Natural Science and Technology, Kanazawa University, Kanazawa, Japan.  
Kien Giang College, 425 Mac Cuu, Vinh Thanh, Rach Gia, Kien Giang, Vietnam  
Email: tlhtrung@kgc.edu.vn

Hiroshi Masuya and Kubo Yoshimori

Faculty of Geoscience and Civil Engineering, Institute of Science and Engineering, Kanazawa University, Japan  
Email: {masuya, ykubo}@se.kanazawa-u.ac.jp

Hiroshi Yokoyama

Research Institute for Infrastructure Engineering, Nippon Engineering Consultants Co., Ltd., Japan  
Email: yokoyama\_hiroshi@ne-con.co.jp

**Abstract**—The use of fiber-reinforced polymer (FRP) bars strengthened reinforced concrete (RC) structures by Near-Surface Mounted (NSM) method plays a key role in the external strengthening and reinforcing of the structures. A series of static tests for RC beams strengthened by FRP NSM method was carried out to identify their effects on the actual response of such RC beams. In all experimental cases, using externally bonded FRP bars to the tensile region of RC beams by NSM method has improved significantly the flexural strength of the beams. Additionally, the numerical simulation had been done to reproduce the behavior of RC beams strengthened by FRP NSM method under static load. The reliable constitutive models and contact conditions were adopted adequately in these models. It was also shown that the numerical simulation result agrees well with the experimental result. Finally, the calculated equations based on the latest codes of design and construction of externally bonded FRP bars are presented in order to verify the flexural strength of the beams under static load.

**Index Terms**—RC beams, FRP bars, NSM method, flexural strength, numerical simulation, static load

## I. INTRODUCTION

Externally bonded fiber-reinforced polymer (FRP) bars have been used to strengthen and reinforce existing concrete structures around the world since the mid-1980s. The number of projects using FRP bars worldwide has increased significantly a few 20 years ago because this reinforcement was developed as an alternative method to traditionally external reinforcing techniques such as steel plate bonding and steel or steel column jacketing. Technique including external post-tensioning and epoxy-bonding steel plates have been applied successfully to increase the strength of slab, beam, and column in existing bridges and buildings. High strength composite

plates are known as an extension of the steel plating method. The advantages of composite materials involved in immunity to corrosion, a low volume to weight ratio, and many delivery shapes.

The main types of fibers used in civil engineering applications are Carbon fiber reinforced polymer (CFRP), Glass fiber reinforced polymer (GFRP), and Aramid fiber reinforced polymer (AFRP). There are companies produced these materials including CarboDur (Sika Corporation), Forca Tow Sheet (Tonen Corporation), and Replark (Mitsubishi). The shape of FRP can be divided into bars, cables, 2-D and 3-D grids, sheet, plates, etc. CFRP material appeared at first to be one of the best approaches for the external strengthening of concrete structures. CFRP is composite materials built from the combination of carbon fiber and the epoxy resin matrix. Therefore, the composite possesses very high strength and elastic modulus in the fiber direction. Its fatigue properties are also outstanding, and the transversal strength of the composite is low, however, this drawback is not relevant for strengthening the application.

The CFRP Forca Tow Sheet was applied on Shirota Bridge in Kyushu province, Japan. Due to relaxing of the allowable loads (from 200 to 250 kN) the stress in flexural and shear reinforcing bars of the bridge slab exceeded the allowable limit of 1200 kg/cm<sup>2</sup>. The CFRP strengthening was designed to reduce the stress below the allowable value. After the reinforcement, the measurements were done with the strain gauges mounted at flexural and shear reinforcing bars. The result attained a substantial decrease in deflection and stress by more than 30 %. To confirm the long-term reinforcing effect, the strain gauges were monitored over one year period. The results clearly indicate that the reinforcing effect is still effective after one year as discussed by A. Naaman [1].

Nowadays, applying the technique of externally bonded FRP bars by Near-Surface Mounted (NSM)

method becomes widespread. There are some studies in terms of this technique performed to survey the static behavior of structures strengthened by FRP bars. Recently, FRPs have replaced steel plates and emerged as a better material for externally strengthen for beams and columns. The members can gain better resistance and protection against environmental conditions [2]. This is a well-accepted technology that is becoming popular among designers and contractors because this technique has improved clearly the flexural and shear performance of concrete structures [3,4]. Two popular types of FRP bars used for NSM method are round bars typically delivered to the site in the form of single bars or in a roll depending on bar diameter; rectangular bars or strip typically delivered to the site in a roll. The discovery of FRP NSM reinforcement open a new trend of research and engineering community because its benefits outweigh any drawbacks. It is easy to install into the grooves by epoxy resin or cement grout which cover effectively FRP bars against environmental impact because epoxy resin or cement grout can be used for its rapid setting and bond strength.

The codes of externally bonded FRP systems have been developed in Europe, Japan, Canada, and the United States. In Europe, the International Federation for Structural Concrete (FIB) published a bulletin on design guidelines for externally bonded FRP bars for RC structures (International Federation for Structural Concrete 2001). In Japan, the Japan Society of Civil Engineers (JSCE), the Japan Concrete Institute (JCI), and the Railway Technical Research Institute (RTRI) published several documents related to the use of FRP bars in concrete structures. The Canadian Standards Association (CSA) have developed guidelines for FRP systems, “Fibres reinforced structures” of Canadian Highway Bridge Design Code was completed in 2006. In the United States, standards for evaluating FRP systems are available to American Concrete Institute (ACI) such as “Guide for the Design and Construction of Externally Bonded FRP Systems for Strengthen Concrete Structures” of ACI 440.2R-08 [5], and “Guide for the Design and Construction of Structural Concrete Reinforced with FRP Bars” of ACI 440.1R-15 [6], ACI 318-05 [7].

This study involves one of the parts in investigating the dynamic and static behaviors of reinforced concrete (RC) structures strengthened by FRP NSM method. Particularly, this paper presents the static tests of strengthened RC beams and normal RC beams. Experimental results are evaluated focusing on cracks patterns, load-displacement relation, load-strain relation, and moment values. The validity of the flexural strength of the beams in experiment is confirmed by comparison with that of numerical results obtained by the programme’s user manual [8] as well as that of theoretical results based on the latest codes of ACI.

## II. OUTLINE OF STATIC EXPERIMENT

### A. Test Specimen Detail

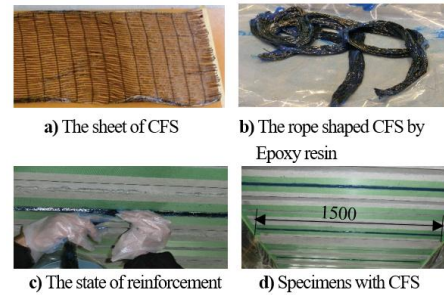


Figure 1. Reinforced method.

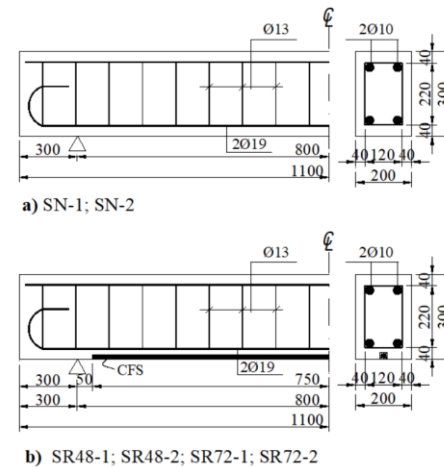


Figure 2. Detail of specimens (Unit: mm).

FRP bars to strengthen RC beams was produced by Forca Tow Anchors (FTA-C1-48-250 and FTA-C1-72-250) of Nippon Steel Sumikin Co., Ltd with initial shape of the sheet as shown in Fig. 1(a). The total number of small strands in the sheet consists of two types, 48 and 72 carbon fiber strands (CFS). There were different stages to strengthen RC beams with the initial shape of fiber as a sheet by NSM method. Firstly, this sheet was mixed with epoxy resin as shown in Fig. 1(b). After that, it was bonded into grooves made on the bottom concrete surface of beams as shown in Fig. 1(c), in which the surface of grooves was prepared carefully as removing all dust and weak concrete. Finally, the FRP bar was buried in the groove as a rectangular bar with a length of 1.5 m (Fig. 1(d)).

Table I and Table II respectively show material properties of FRP bar and reinforcing bars, and Fig. 2 illustrates the detail of RC beams and the arrangement of reinforcing bars. The beam shown in Fig. 2(a) is normal RC beams (SN1 and SN2) without the reinforcement of FRP NSM method. The beams shown in Fig. 2(b) are RC beams with the reinforcement of NSM FRP of which names are SR48-1, S48-2 and S72-1, S72-2. They were strengthened with 48 and 72 strands respectively by NSM method. After strengthening, the cross sections of 48 and 72 strands were  $44 \text{ mm}^2$ ,  $66 \text{ mm}^2$  respectively. All of the sections of concrete was rectangular with a wide of 200 mm, and a height of 300 mm. The length of specimens

was 2200 mm. Main reinforcing bars of diameter 10 mm (D10) and 19 mm (D19) were arranged at upside and down side, respectively. The stirrups of diameter 13 mm (D13) were used. The span length of beams was 1600 mm and the length of FRP bars was 1500 mm.

TABLE I. MATERIAL PROPERTIES OF FRP

Name	48 CFS	72 CFS
The total number of strands	48	72
Cross section (mm <sup>2</sup> )	44	66
Young modulus (GPa)	237	237
Fineness - g - (g/km)	1650	1650
The number of filaments - K	24	24
Typical density (g/cm <sup>3</sup> )	1.8	1.8
Ultimate tensile strength (MPa)	3990	3990

TABLE II. MATERIAL PROPERTIES OF REINFORCING BARS

Name	D10	D13	D19
Yield strength (MPa)	295	295	345
Tensile strength (MPa)	431	431	494

The loading test was performed to confirm the static behavior of RC beams strengthened by FRP bar and normal beams as shown in Fig. 3. A 3000 kN hydraulic jack and one load cell were placed the middle of span for applying and measuring the imposed loading. In order to obtain the deflection properties of the entire specimen, displacement meters were installed vertically at the loading position. Furthermore, strain gauges were also installed to confirm the strain variation of concrete, steel and FRP bar.

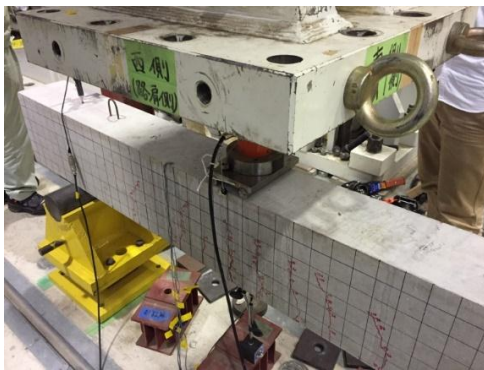


Figure 3. Static loading Experiment.

**B. Experimental Results**

Fig. 4 presents the crack patterns of specimens. From the figures, it can be seen that the crack patterns of the tested beams under static load have shifted from vertical (flexural) cracks to diagonal (shear) cracks. Most flexural cracks occurred around the bottom of the specimens; conversely, the formation of shear cracks appeared far away from the position of applied load and next to supports. It means that failures of all beams tested under static load were governed by both flexural and shear modes. In addition, the crack patterns of both RC beams strengthened by FRP NSM method and normal RC beams were distributed in two-thirds from the middle span of the beams, and the difference in distributed cracks was very small. These cracks were observed carefully for all beams,

their widths developed gradually when increasing the static load and their lengths extended from the bottom to the top of the beams. However, the crack patterns of SR48-1, SR48-2, and SR72-1 exhibited smaller width and shorter length of flexural crack than normal beams when surveying at the center of beams. It can be said that the strengthening of FRP by NSM method can lead to effective resistance to the expansion of cracks.

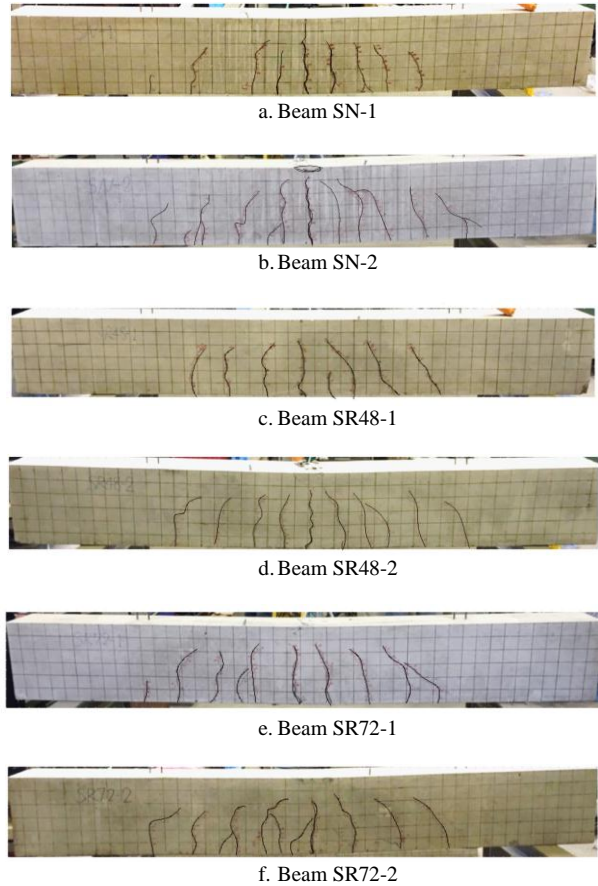


Figure 4. Distribution of cracks under static load.

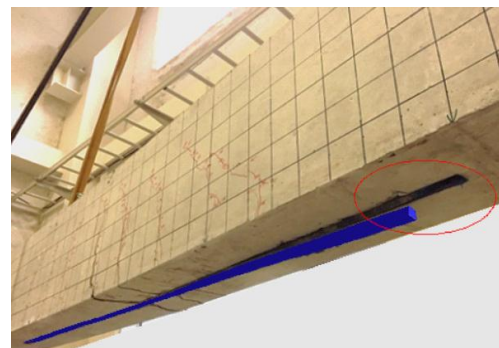


Figure 5. Separation of FRP, beam SR48-1.

It is also interesting to note that the strengthened beams (SR48-1 and SR48-2) finally discontinued due to peeling of FPR bars from the substrate as shown in Fig. 5. The occurrence of bonding failure at the epoxy-concrete interface in terms of the specimens strengthened by FRP NSM method is difficult to control when the load is applied until the ultimate stage.

The relationships between load and displacement in static experiments are shown in Fig. 6. At the early stage of loading, the slope of curves of these beams was almost the same, which means that the contribution of FRP bars had not been activated yet. When the applied load was higher than 130 kN, the behavior of SN-1 and SN-2 no longer performed linear elastic stage because of the yield

of rebars. While, the strengthened beams remained linear elastic behavior until the applied load over 150 kN. As expected, the beams strengthened by FRP bars performed better the flexural strength than the normal beams, especially for beam SR48-1 because this is one of strengthened beams exhibited high bending capacity with minimum displacement.

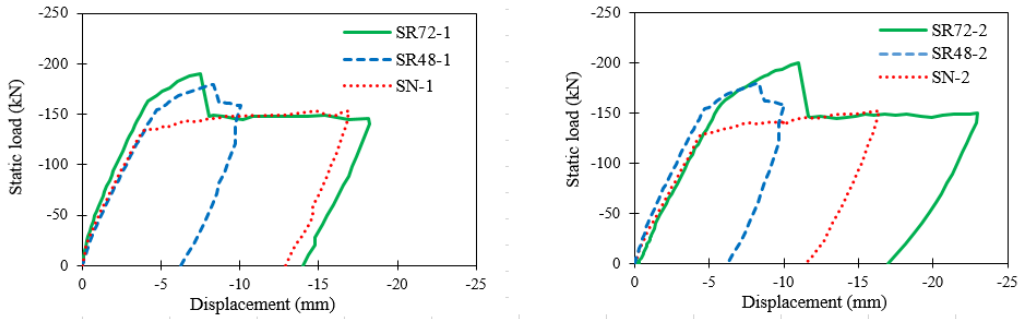


Figure 6. Static load-displacement relationship of experiment.

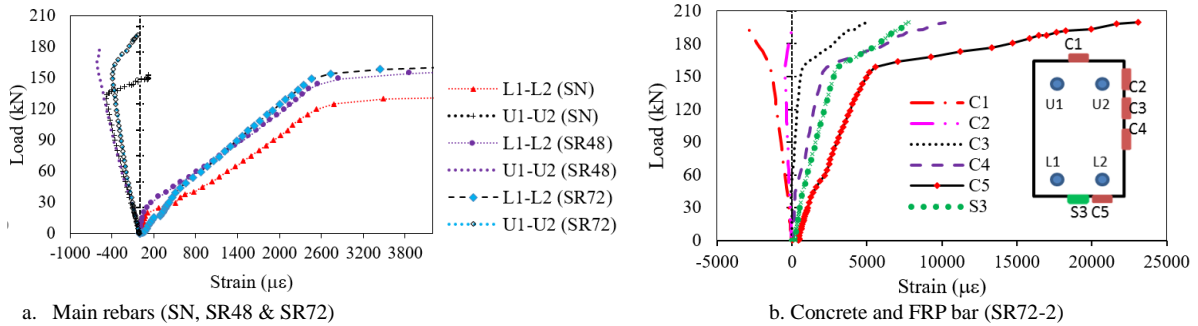


Figure 7. Load-strain relationships

Table III presents the yield loads and maximum loads in the experiment, where the range of maximum load of SR48 and SR72 is from 179 kN to 199 kN. While, the maximum load of SN2 and SN1 are 151 kN and 153 kN, respectively. Therefore, the increase in the maximum load of the strengthened beams is from 1.18 to 1.31 times compared with the normal beams. As a result, the flexural strength of the beams strengthened by FRP NSM method is greater than that of normal RC beams under static load. Moreover, it has become clear that an increase in the number of strands of FRP bars can leads to an increase in the flexural strength of RC beams.

TABLE III. EXPERIMENTAL RESULTS

Specimens	Yield load (kN)	Maximum load (kN)
SN-1	134	153
SN-2	134	151
SR48-1	155 (155/134=1.16)	179 (179/152=1.18)
SR48-2	160 (160/134=1.19)	188 (188/152=1.24)
SR72-1	163 (163/134=1.22)	190 (190/152=1.25)
SR72-2	165 (165/134=1.23)	199 (199/152=1.31)

Fig. 7 shows the strain results of main rebars, concrete, and FRP bar obtained from the experiment. The strain results at each position of the main rebars shown in Fig. 7(a) is the average values of strain gauges obtained from similar specimens. Overall, the variation of strain at the

observed positions (L1, L2, U1 and U2) shows similar tendencies in both the cases without (SN) and with (SR48 and SR72) the use of FRP NSM method. Particularly, the strain of main rebars at the bottom region of cross-section (positions L1 and L2) performed tensile behaviors; whereas the top region (positions U1 and U2) showed compressive behaviors when the load was applied to the specimens.

From Fig. 7(a), the bottom rebars L1 and L2 performed yielding behavior when the applied load were 134 kN, 157 kN, and 164 kN for SN, SR48 and SR72, respectively. The corresponding strain values were measured to be about 2092  $\mu\epsilon$ , 2185  $\mu\epsilon$ , and 2074  $\mu\epsilon$ . Thus, the increase in the yield load is from 1.16 to 1.23 times, the difference in the obtained strain values is minimal. It can be noted that the presence of FRP bar leads to such a positive result for the yield of the main rebars at the bottom of the strengthened beams SR48 and SR72. In addition, positions U1 and U2 where compressive state occurred initially, and then this state became tensile direction because the neutral axis at the cross-section tended to shift the upper region as the load increased.

In addition, the strains of concrete and FRP bar were also observed at the midspan of beam SR72-2 as shown in Fig. 7(b). The strain of concrete at midspan was

measured in both compressive region (C1 and C2) and tensile region (C3, C4 and C5). As can be seen the tensile strain of concrete turned into rapidly growing when the load was applied, which caused the crack patterns as shown in Fig. 4. In terms of the results calculated from the strain of concrete, the strains was  $1582 \mu\epsilon$  in compression (position C1), and  $7074 \mu\epsilon$  in tension (position C5). The neutral axis depth of the beam assumed the linear distribution of strain in the cross-section is approximately 55 mm at 163 kN.

Regarding the tensile deformation of FRP bar at position S3, the maximum tensile strain was measured to be  $\sim 7788 \mu\epsilon$  at the final loading level ( $P_{max} = 199$  kN) and the corresponding tensile stress was estimated to be  $1845.76 \text{ N/mm}^2$ , which is equivalent to about 46% of the ultimate tensile stress of FRP bar used ( $3990 \text{ N/mm}^2$ ). From this obtained result, it can be confirmed that the tensile capacity of FRP bar strengthened RC beam by NSM method can achieve nearly half its tensile capacity in design under ultimate load.

### III. NUMERICAL SIMULATION

#### A. Constitutive Model

The numerical simulation had been done to reproduce the static behavior of RC beams with and without the strengthening of FRP NSM method. It would be possible to study the static behavior of general structure by analysis. Finite element model (FEM) of the beams is illustrated in Fig. 8. This 3D model was built by various type of elements, and the concrete was meshed into 11400 eight-node solid elements with a size of 25 mm. Besides the beam elements were applied to model reinforcing bars, shell elements were modelled the applied load. Moreover, solid elements were adopted to model FRP bars which were designed to the cross section of  $44 \text{ mm}^2$  and  $66 \text{ mm}^2$  for beams SR48 and SR72, respectively.

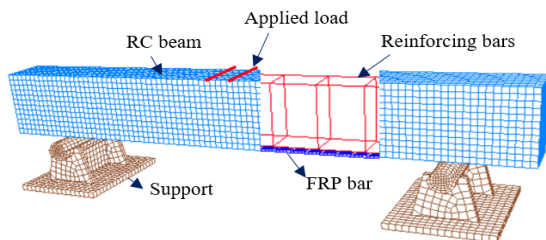


Figure 8. Technical sketch of the RC beam built in LS-DYNA

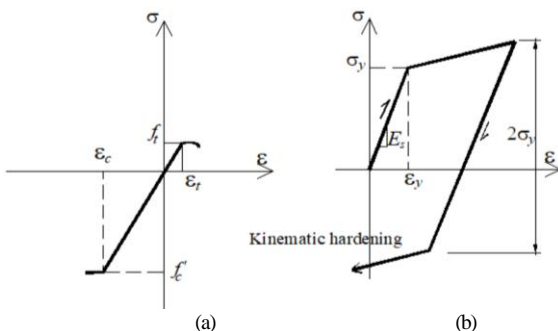


Figure 9. Stress - strain relations of (a) concrete and (b) reinforcing bars

LS\_Dyna provides a number of the constitutive models (e.g. MAT 16, 25, 72, 84/85, 145 and 159) to model the concrete behavior under static, impact and blast loads. Some of these available models and their verification has been published [9,10,11]. In this study, the material model \*Mat\_Concrete\_Damage\_Rel3 (MAT\_72\_REL3) was used to simulate the complex behavior of concrete, and the stress-strain relationship of concrete is shown in Fig. 9(a). This constitutive significantly estimates the post-elastic bulk modulus for compression and a linear model for tension [8]. Mass density  $\rho = 2500 \text{ kg/m}^3$ , Young's modulus  $E = 28.43 \text{ MPa}$ , Poisson's ratio  $\nu = 0.167$ , compressive strength  $f'_c = 35.81 \text{ MPa}$  and tensile strength  $f'_t = 2.81 \text{ MPa}$  were used for the mechanical properties of concrete.

Regarding the constitutive model of reinforcing bars, an elastic-plastic material model called "Mat Piecewise Linear Plasticity" (MAT 24) was adopted to model the reinforcing bars. The kinematic hardening behavior was considered in this model, which is predicted the yield surface remains constant in size and translates in the direction of yielding [8] as shown in Fig. 9(b). The yield strength of reinforcing bars is shown in Table II. Mass density  $\rho = 7850 \text{ kg/m}^3$ , Young's modulus  $E = 210 \text{ MPa}$ , Poisson's ratio  $\nu = 0.3$  were used for steel material. In addition, the constitutive model of FRP bars was shown as elastic behavior via experimental observation. Therefore, the LS-DYNA material model named "Mat Elastic" (MAT 001) was selected, in which the ultimate strength  $f_u$ , strain  $\epsilon_u$  and Young's modulus  $E$  are  $3990 \text{ MPa}$ ,  $0.0168 \text{ m/m}$  and  $237 \text{ GPa}$ , respectively.

#### B. Contact Conditions

This model consists of different components including concrete, reinforcing bars, FRP bar, supports and applied load. Therefore, the precise reproduction of contact behavior between those components can be an essential factor. The interactions used in the models were divided into two following groups. (1) Automatic surface to surface, assigned for reaction between applied load and concrete, support and concrete; (2) Automatic surface to surface tiebreak, contacted between concrete and FRP bar. On the other hand, the method of incorporating reinforcing bars into the concrete was described by Constrained Lagrange in Solid technique [8].

The LS-DYNA contact algorithm named "Contact Automatic Surface to Surface" is employed to simulate the contact between the applied load and the beam, and between the supports and the beam. This technique allowed creating pairs of surfaces that can connect the nodes on the surfaces together during the analysis. Moreover, the technique "Constrained Lagrange in Solid" effectively addresses penalty coupling of beams to solid elements [8], in which the beam elements of reinforcing bars were modeled the slave and the solid elements of concrete was modeled the master. "Tiebreak Contact" is used to model the slip relationship between concrete and FRP bar. The tiebreak allowed the separation of the surfaces under tensile load by setting the parameters of tensile failure strength (NFLS) and shear failure strength

(SFLS). These parameters were typical properties for epoxy adhesives. In this simulation, NFLS = 56 MPa, and SFLS = 44 MPa were applied [12].

#### IV. FLEXURAL STRENGTH

The most important mechanism of load transfer is the flexural strength, so an understanding of the detailed requirements of calculation procedure is necessary. Externally bonding FRP bars by NSM method to the tension area of RC beams will increase significantly the ultimate flexural strength of RC beams under static load. In this study, the flexural strength of the beams is also calculated by the codes of ACI [5, 6, 7].

##### A. Assumptions in the Computation of Flexural Strength.

The simple assumptions involve in principles of force equilibrium, strain compatibility, constitutive laws of the materials, and make reference to the codes of ACI [5]. The computation of the flexural strength of a cross section with an external application of FRP NSM reinforcement has used the assumptions as follows:

- The computation is based on dimensions, the arrangement of reinforcing bars, and constitutive laws of concrete, steel, and FRP bars;
- The equilibrium between tensile forces (in steel and FRP bars) and compressive forces (in concrete) always remains;
- There is no bonding failure between external FRP bars and the concrete substrate;
- The stress-strain relationship of FRP bars is linear elastic.

The constitutive of material models are assumed as bellows. Firstly, regarding the stress-strain relationship for concrete in compression as shown in Fig. 10(a), the slope of the initial part of the diagram is reasonably constant. When the stress increases gradually, the relationship become nonlinear elastic until the peak occurs where very little extra stress causes a large increase in strain. The peak in stress is known as the compressive strength of concrete ( $f'_c$ ) and the corresponding compressive strain is denoted ( $\epsilon'_c$ ). At a certain ultimate strain ( $\epsilon_{cu}$ ) the concrete crushes regardless of the level of stress. The maximum usable compressive strain in the concrete is assumed to 0.003.

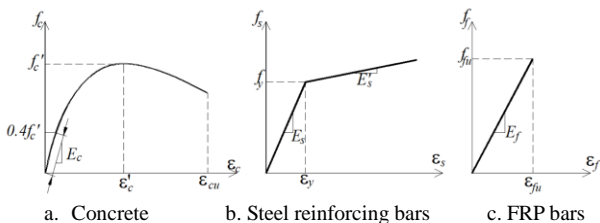


Figure 10. Stress-strain relationship

Secondly, regarding the stress-strain relationship of reinforcing bars as shown in Fig. 10(b), the elastic modulus ( $E_s$ ) is equal to the slope of the linear portion. ACI 440. 2R-08 allows a mean value of 200.000 N/mm<sup>2</sup>

to be assumed for  $E_s$ . The modulus in the plastic region is set as  $E'_s = 0.01E_s$  [4]. The ultimate stress is assumed as follows:

$$f_s = E_s \epsilon_s \text{ for } \epsilon_s \leq \epsilon_y \tag{1}$$

$$f_s = f_y + E'_s (\epsilon_s - \epsilon_y) \text{ for } \epsilon_s \geq \epsilon_y \tag{2}$$

where  $f_y$ - $\epsilon_y$  and  $f_s$ - $\epsilon_s$  are stress-strain in the reinforcing bars at yielding and ultimate stage, respectively.

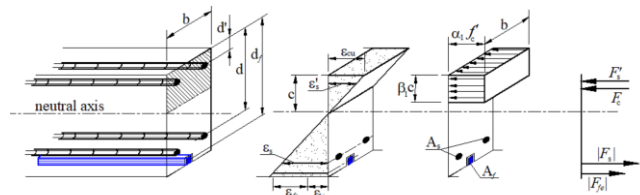
Finally, the stress-strain curve of FRP bar as shown in Fig. 10(c) is assumed linear elastic. The material properties are reported by manufacturers including the ultimate tensile strength ( $f_{fu}^*$ ) and the ultimate rupture strain ( $\epsilon_{fu}^*$ ) that typically do not consider long-term exposure to environmental conditions. Therefore, calculating the ultimate tensile strength and rupture strain is used according to the recommendation of environmental reduction factor ( $c_E$ ) as shown in Table IV.

$$f_{fu} = c_E f_{fu}^* \tag{3}$$

$$\epsilon_{fu} = c_E \epsilon_{fu}^*$$

##### B. The Flexural Strength of Rectangular Section

The distribution of strain and stress for the rectangular section under static load is illustrated in Fig. 11. The different forces act on an RC section in sag region include the compression ( $F_c$ ) of concrete above the neutral axis ( $c$ ), the tension ( $F_s$ ) and compression ( $F'_s$ ) of reinforcing bars, the tension ( $F_{fe}$ ) of FRP bars.



a. Section b. Strain distribution c. Stress block d. Axis force

Figure 11. Stress-strain distribution for a rectangular section

TABLE IV. ENVIRONMENTAL-REDUCTION FACTOR  $C_E$

Exposure condition	Fiber type	$C_E$
Interior exposure	Carbon	0.95
	Glass	0.75
	Aramid	0.85
Exterior exposure (bridges, piers and unenclosed parking garages)	Carbon	0.85
	Glass	0.65
	Aramid	0.75
Aggressive environment (chemical plants and wastewater treatment plants)	Carbon	0.85
	Glass	0.50
	Aramid	0.70

By equilibrium, the sum of the compressive forces have to equal zero, that is:

$$F_c + F'_s - F_s - F_{fe} = 0 \tag{4}$$

Therefore,

$$\alpha_1 f_c' \beta_1 c d + A_s' f_s' - A_s f_s - A_f f_{fe} = 0 \quad (5)$$

where  $A_s, f_s$  are the area and stress of the tensile area of reinforcing bars,  $A_s', f_s'$  are the area and stress of the compressive area of reinforcing bars,  $A_f, f_{fe}$  are the area and effective stress of FRP bars,  $b$  is width of compression face of beam. The concrete stress block factors ( $\alpha_1, \beta_1$ ) relate to the depth of equivalent rectangular stress block and depth of neutral axis depth ( $c$ ). ACI 381-05 calculates the factors based on the parabolic stress-strain relationship for concrete as follows:

$$\beta_1 = \frac{4\varepsilon_c' - \varepsilon_c}{6\varepsilon_c' - 2\varepsilon_c} \quad (6)$$

$$\alpha_1 = \frac{3\varepsilon_c' \varepsilon_c - \varepsilon_c^2}{3\beta_1 \varepsilon_c'} \quad (7)$$

where ( $\varepsilon_c'$ ) is strain corresponding to the compressive strength of concrete ( $f_c'$ ) calculated as follows:

$$\varepsilon_c' = \frac{1.7 f_c'}{E_c} \quad (8)$$

An assumption of the depth to neutral axis ( $c$ ) is described by a trial-and-error method (ACI 440.2R-08). The initial assumption of neutral axis ( $c$ ) is  $0.2d$  ( $d$  is distance from extreme compression to the centroid of tension reinforcement) to calculate the level of strain and stress corresponding to concrete, steel and FRP bar, and to check the internal force equilibrium afterward. If the result is different with the initial assumption, the calculation procedure needs to be repeated by using the revised assumption.

For any assumption of the depth to the neutral axis, the strain level in concrete ( $\varepsilon_c$ ) the tensile ( $\varepsilon_s$ ) and compressive ( $\varepsilon_s'$ ) strain of reinforcing bars, and FRP bar ( $\varepsilon_{fe}$ ) can be calculated by similar triangles as follows:

$$\varepsilon_c = (\varepsilon_{fe} + \varepsilon_{bi}) \left( \frac{c}{d_f - c} \right) \quad (9)$$

$$\varepsilon_{fe} = \varepsilon_{cu} \left( \frac{d_f - c}{c} \right) - \varepsilon_{bi} \leq \kappa_m \varepsilon_{fu} \quad (10)$$

$$\varepsilon_s = (\varepsilon_{fe} + \varepsilon_{bi}) \left( \frac{d - c}{d_f - c} \right) \quad (11)$$

$$\varepsilon_s' = \varepsilon_{cu} \left( \frac{c - d'}{c} \right) \quad (12)$$

where  $\kappa_m$  is a bond dependent coefficient to limit the strain in the FRP reinforcement, and ACI 440.2R-08 allows a value of  $\kappa_m$  from 0.6 to 0.9.  $\varepsilon_{fu}$  is the design rupture strain of FRP bars,  $d_f$  is the effective depth of FRP bars,  $d'$  is the distance from extreme compression to

the centroid of compression reinforcement. The initial strain level on bonded substrate ( $\varepsilon_{bi}$ ) can be determined from the moment of dead loads ( $M_{DL}$ ) and second moment of inertia ( $I_{cr}$ ) as shown in (13).

$$\varepsilon_{bi} = \frac{M_{DL} (d_f - k.d)}{I_{cr} E_c} \quad (13)$$

Here,

$$k = \sqrt{2\rho n + (\rho n)^2} - \rho n \quad (14)$$

$$\rho = \frac{A_s}{bd}; n = \frac{E_s}{E_c} \quad (15)$$

where  $k$  is the ratio of the depth of neutral axis to reinforcement depth measured from extreme compression fiber,  $n$  is the modular ratio of elasticity between steel and concrete,  $\rho$  is reinforcement ratio,  $b$  is width of compression face of the member.

The moment-curvature distribution of RC beams strengthened by FRP NSM method can be classified into three cases. Firstly, the cracking moment ( $M_{cr}$ ) is given by (16), where the gross second moment ( $I_g$ ) neglects presence of reinforcement. Secondly, yielding moment ( $M_y$ ) involves in the stress curve of reinforcing bars that is not beyond the yield stress yet as shown in (17). Finally, maximum moment ( $M_n$ ) occurs at the post-yielding stage as shown in (18). Calculation for these moments is respectively based on the equilibrium of all forces as follows:

$$M_{cr} = \frac{0.62 \sqrt{f_c' I_g}}{y_t} \quad (16)$$

$$M_y = A_s f_y \left( d - \frac{\beta_1 c}{2} \right) + \psi_f A_f f_{fe} \left( d_f - \frac{\beta_1 c}{2} \right) - A_s' f_s' \left( d' - \frac{\beta_1 c}{2} \right) \quad (17)$$

$$\phi M_n = \phi \left[ A_s [f_y + E_s' (\varepsilon_s - \varepsilon_y)] \left( d - \frac{\beta_1 c}{2} \right) + \psi_f A_f f_{fe} \left( d_f - \frac{\beta_1 c}{2} \right) - A_s' f_s' \left( d' - \frac{\beta_1 c}{2} \right) \right] \quad (18)$$

where  $y_t$  is the distance from centroid axis of the gross section to tension face,  $\psi_f$  is an addition reduction factor of 0.85 recommended to take into account for the strength contribution of FRP bars (ACI 440.2R-08). The strength reduction factor ( $\phi$ ) is given by (19).

$$\phi = \begin{cases} 0.9 \text{ for } \varepsilon_s \geq 0.005 \\ 0.65 + \frac{0.25(\varepsilon_s - \varepsilon_y)}{0.005 - \varepsilon_y} \text{ for } \varepsilon_y < \varepsilon_s < 0.005 \\ 0.65 \text{ for } \varepsilon_s \leq \varepsilon_y \end{cases} \quad (19)$$

V. VERIFICATION AND DESIGN

A. Comparison of Results

Fig. 12 shows the relations of static load to displacement in the experiment (Exp) and numerical simulation (FEM) Overall, the curves and values of yield load and maximum load were in good agreement for all cases. Regarding normal RC beam, the yield and maximum load of the simulation are 136 kN and 150 kN respectively, which is approximately experimental values. The displacement peaks at around 16 mm for both

simulate and experiment. It became clear that the static behavior of model SN in simulation is similar that of the test. In addition, the results of models SR48 and SR72 also tend to be similar together. The maximum load of SR48 in simulation ( $P_{max} = 180$  kN) is 4.3 % smaller than that of experiment ( $P_{max} = 188$  kN for SR48-2), and the maximum load of SR72 in simulation ( $P_{max} = 192$  kN) is 3.5 % smaller than that of experiment ( $P_{max} = 199$  kN for SR72-2). The deviations of maximum loads are minimal when comparing between experimental and numerical values.

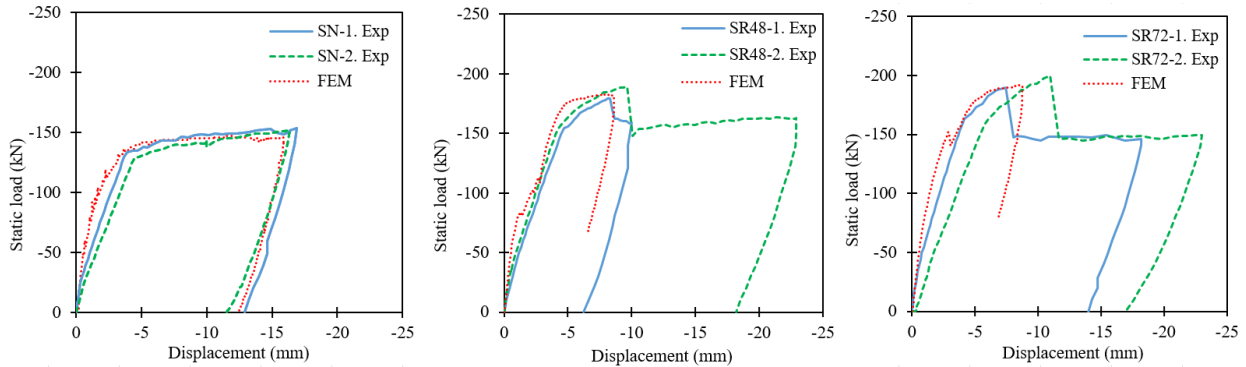


Figure 12. Load - displacement relationship

TABLE V. COMPARISON OF EXPERIMENTAL AND THEORETICAL RESULTS

Specimens		SR48-1	SR48-2	SR72-1	SR72-2
Yielding Moment (kN • m)	Experiment	58.13	60.00	61.13	61.88
	Theory	58.35	58.35	66.20	66.20
	Simulation by FEM	61.88	61.88	63.75	63.75
	(Experiment-Theory)/Theory (%)	-0.39	2.83	-7.67	-6.53
	(Simulation-Theory)/Theory (%)	6.04	6.04	-3.70	-3.70
Maximum Moment (kN • m)	Experiment	67.13	70.50	71.25	74.63
	Theory	67.98	67.98	75.75	75.75
	Simulation by FEM	67.50	67.50	72.00	72.00
	(Experiment-Theory)/Theory (%)	-1.26	3.71	-5.94	-1.49
	(Simulation-Theory)/Theory (%)	-0.71	-0.71	-4.95	-4.95

Table V compares the values of yielding moment and maximum moment for specimens computed from experiment, numerical simulation and theory. The experimental and numerical values are evaluated by the schematic of the applied load with  $M_n = 0.235Pl$  ( $l = 1600mm$ ) and the theoretical values are calculated by the code of ACI (the maximum moment of beam SR48 is shown in appendix A). For the yielding moment, the discrepancy between experimental and theoretical results ranges from 0.39 % to 7.67 % and between simulation and theory accounts for from 3.7 % to 6.04 %. While, this discrepancy tends to be less for the maximum moment, nearly from 1.26 % to 5.94 % between experiment and theory, and from 0.71 % to 4.95 % between simulation and theory. It can be said that the calculated equations in this study can predict the static ultimate flexural strength of RC beams strengthened by FRP NSM method with relatively high accuracy, and the results of experiment and numerical simulation are reliable as well.

When comparing the calculated values, a small error of under 8% can be explained by the initial assumptions.

While some of these initial assumptions are necessary for the sake of computational ease, the assumptions do not accurately reflect the true fundamental behavior of FRP bars by NSM method. In the experimental procedure, bonding failure at the epoxy-concrete interface caused the separation between the FRP bars and the substrate of concrete as shown in Fig. 5. Whereas the initial assumption did not consider such a separation.

B. Applicability for Design

The design flexural strength of the beams ( $M_n$ ) is required exceedingly the factored moment ( $M_u$ ) as indicated by (20). The design flexural strength refers to the nominal strength of the beams multiplied by a strength reduction factor ( $\phi$ ) as shown in (19), and the factored moment ( $M_u$ ) at a section refers to the moment calculated from the dead-load moment ( $M_{DL}$ ) and live-load moment ( $M_{LL}$ ) given by (21).

$$\phi M_n \geq M_u \tag{20}$$

$$M_u = 1.1M_{DL} + 0.75M_{LL} \quad (21)$$

NSM method consists of installing rectangular or circular FRP bars in a groove cut into the concrete surface and bonded in place using an adhesive as shown in Fig. 13. The groove should be dimensioned to ensure adequate adhesive around the bars, and typical groove dimensions for various types of FRP bar are referred to [2]. For FRP round bars, the minimum dimension of the grooves should be taken at least 1.5 times the diameter of

the FRP bars. For FRP rectangular bars, the minimum size of groove is  $3.0a_f \times 1.5b_f$  ( $a_f$ ,  $b_f$  are the width and height of FRP bar). The space of grooves for FRP bars should be greater than twice the depth of the groove to avoid overlapping of the tensile stresses around the FRP bars. In addition, a clear edges distance of four times the depth of the NSM groove should be provided to minimize the debonding failure of FRP bars [6]. Flowchart to design FRP NSM reinforcement for the beams is shown in Fig. 14.

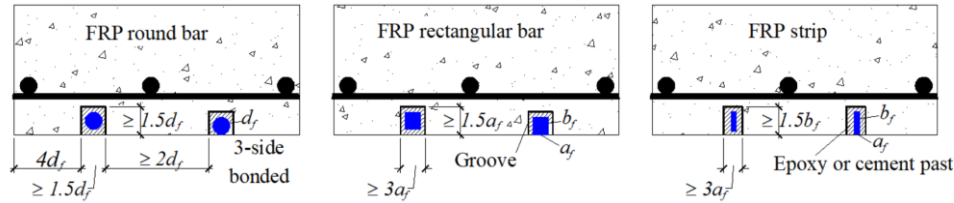


Figure 13. Variety of NSM FRP bars and minimum dimensions of grooves

TABLE VI. PHYSICAL PROPERTIES OF FRP SYSTEM

Properties	GFRP	CFRP	AFRP
Typical density ( $\rho$ ) g/cm <sup>3</sup>	1.25 to 2.10	1.50 to 1.60	1.25 to 1.40
Tension strength ( $f_{fu}^*$ ) Mpa	483 to 690	600 to 3690	1720 to 2540
Elastis modulus ( $E_f$ ) $\times 10^3$ Gpa	35.0 to 51.0	120.0 to 580.0	41.0 to 125.0
Rupture strain, percent	1.2 to 3.1	0.5 to 1.7	1.9 to 4.4

The physical properties of materials made FRP bars are summarized in Table VI. In this study, these properties are referred to the Tonen Corporation including density ( $\rho$ ) of 1.8 g/cm<sup>3</sup>, tensile strength ( $f_{fu}^*$ ) of 3990 MPa, strain ( $\epsilon_{fu}^*$ ) of 0.0168 mm/mm and modulus of elasticity ( $E_f$ ) of 237 GPa corresponding to Forca Tow Anchors (FTA-C1-48-250 and FTA-C1-72-250) of Nippon Steel Sumikin Co., Ltd. The area of FRP bars is given by (22), where  $g$  is fineness and  $n'$  is the number of strands per a sheet.

$$A_f = \frac{g \cdot n}{\rho} \times 1000 \quad (22)$$

When calculating the area ( $A_f$ ) of externally bonded FRP bars, its initial assumption can be  $0.333b$  ( $b$  is the width of the cross section). The length of FRP bar depends on many factors such as cross-sectional shape, dimensions, and material properties. The equilibrium condition of FRP bars with an embedded length involves its developed length ( $l_d$ ). According to a triangular stress distribution, the average bond strength ( $\tau_b$ ) can be half of the maximum bond strength ( $\tau_{max}$ ). Average bond strength for FRP bars can range from 3.5 to 20.7 MPa [6], the following equations for development length can be given:

$$l_d = \frac{d_f}{4(\tau_b)} f_{fe} \quad \text{for round bars} \quad (23)$$

$$l_d = \frac{a_f \times b_f}{2(a_f + b_f) \tau_b} f_{fe} \quad \text{for rectangular bars} \quad (24)$$

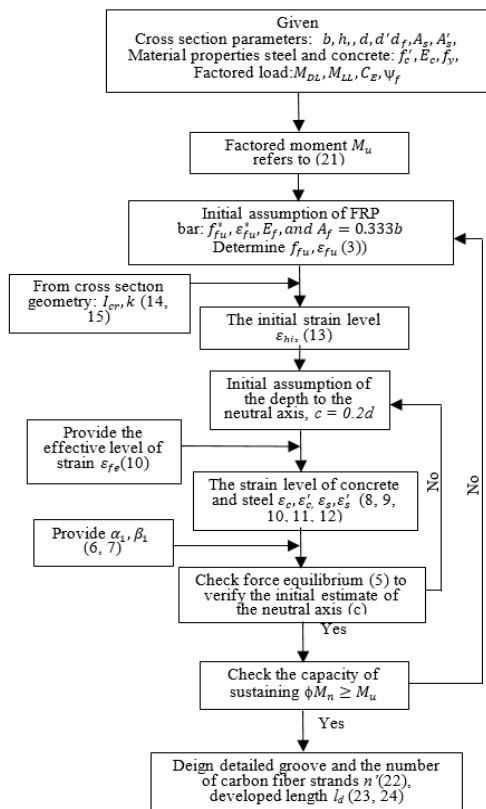


Figure 14. General flowchart for application of design

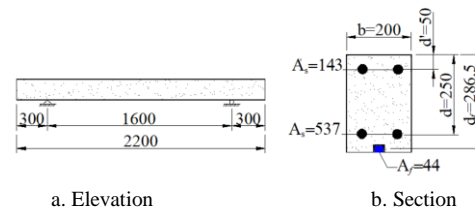


Figure 15. Schematic of the idealized simply supported beam with FRP bar. Unit: N, mm

TABLE VII. MATERIAL PROPERTIES

Material	Fiber type	Value	Unit
Concrete	Compressive strength of concrete, $f'_c$	35.81	N/mm <sup>2</sup>
	Young modulus, $E_c$	28.43	kN/mm <sup>2</sup>
Steel	The strain of yielding stage, $f_y$	345	N/mm <sup>2</sup>
FRP (48 carbon fiber strands)	Ultimate tensile strength, $f_{fu}^*$	3990	N/mm <sup>2</sup>
	Rupture strain, $\epsilon_{fu}^*$	0.0168	mm/mm
	Modulus of elastic $E_f$	237	kN/mm <sup>2</sup>

VI. CONCLUSIONS

In this study, the static behavior of RC beams with and without the strengthening of FRP NSM method performed in experimental and numerical models. In addition, the equations have been shown based on the latest codes in order to calculate the flexural strength of the beams. The achievements of research are summarized as follows:

- It has been concretely shown that externally bonded FRP bars to the tensile region of RC beams by NSM method has enhanced clearly in the flexural strength, and resisted to the expansion of cracks under static loading condition
- Beam SR48-1 is one of the reinforced beams performed the clearest linear elastic behavior until the applied load over 150 kN
- The use of FRP bar can create positive influence on the yield of the main rebars at the bottom of the strengthened beams SR48 and SR72
- The tensile capacity of FRP bar strengthened RC beam by NSM method can achieve nearly half its tensile capacity in design under ultimate load
- The assumptions involved the constitutive models and contact conditions of the components of the beams were adopted adequately in numerical simulation
- Numerical simulation results agreed fairly well with experimental results, and this constituted an effective and reliable design tool in order to study the static behavior of general structures based on these analyses
- The flexural strength of RC beams strengthened FRP NSM method can be calculated accurately by the use of two guides published by ACI
- When comparing the yield and maximum moment values of the beams, the values calculated from experiment, theory and simulation is less than 8 %.
- The flowchart for application of design is shown based on the code of ACI with the addition of calculating the number of strands of FRP bars for the implementation by NSM method

This research contributes a better understanding of the influence of FRP NSM method on the static behaviors of RC beams. This study is considered to be preliminary in reference to the use of numerical models for replacing or modifying the parameters of the full-scale tests with

externally bonded FRP systems. Additionally, the results of the study are also premise to conduct further studies for impact issues in terms of different velocity levels and various strengthened methods on RC structures.

APPENDIX A. The flexural strength of beam SR48

Example illustrates the design of flexural strength of RC beam strengthened by 48 CFS by NSM method as shown in Fig. 15 and material properties are described in Table VII. The steps of calculation are presented as follows:

1. Determining the design values of FRP bar by the use of environmental reduction factor as shown in Table 1, where  $C_E = 0.95$

$$f_{fu} = C_E f_{fu}^* = 0.95 \times 3990 = 3790.5 \text{ N/mm}^2$$

$$\epsilon_{fu} = C_E \epsilon_{fu}^* = 0.95 \times 0.0168 = 0.0159 \text{ mm/mm}$$

2. Calculating the initial strain level on the bonded substrate ( $\epsilon_{bi}$ ) by (13). The analysis of cracked section relates to  $k = 0.329$ ,  $I_{cr} = 167 \times 10^6 \text{ mm}^4$  and the dead-load moment ( $M_{DL}$ ) is 29 kN·m

$$\epsilon_{bi} = \frac{M_{DL} (d_f - k.d)}{I_{cr} E_c} = \frac{29 \times 10^6 (286.5 - 0.329 \times 250)}{167 \times 10^6 \times 28.430}$$

$$\Rightarrow \epsilon_{bi} = 0.0012 \text{ mm/mm}$$

3. Assuming initially the depth to the neutral axis,  $c = 0.2d = 0.2 \times 250 = 50 \text{ mm}$ , this value is adjusted after checking equilibrium.
4. Confirming the effective level of strain in the FRP bar by (10), where the dimensionless bond-dependent coefficient for flexural,  $\kappa_m = 0.6$

$$\epsilon_{fe} = \epsilon_{cu} \left( \frac{d_f - c}{c} \right) - \epsilon_{bi} = 0.003 \left( \frac{286.5 - 50}{50} \right) - 0.0012$$

$$= 0.0129 \text{ mm/mm} > \kappa_m \epsilon_{fu}$$

$$(\kappa_m \epsilon_{fu} = 0.6 \times 0.0159 = 0.0096 \text{ mm/mm})$$

$$\text{Hence, } \epsilon_{fu} = 0.0096 \text{ mm/mm}$$

5. Determining the level of strains in concrete and reinforcing bars by (9, 11, 12).

$$\epsilon_c = (\epsilon_{fe} + \epsilon_{bi}) \left( \frac{c}{d_f - c} \right) = (0.0096 + 0.0012) \left( \frac{50}{286.5 - 50} \right)$$

$$= 0.0023 \text{ mm/mm}$$

$$\epsilon_s = (\epsilon_{fe} + \epsilon_{bi}) \left( \frac{d - c}{d_f - c} \right) = (0.0096 + 0.0012) \left( \frac{250 - 50}{286.5 - 50} \right)$$

$$= 0.0092 \text{ mm/mm}$$

$$\epsilon'_s = \epsilon_{cu} \left( \frac{c - d'}{c} \right) = \left( \frac{50 - 50}{50} \right) = 0$$

6. Determining the level of stress the reinforcing bars and FRP bar from Hooke's law:

$$f_s = E_s \times \varepsilon_s = 200,000 \times 0.0092 = 1830.6 \text{ N/mm}^2$$

$$\Rightarrow f_s > f_y = 345 \text{ N/mm}^2$$

$$f_{fe} = E_{fe} \times \varepsilon_{fe} = 237,000 \times 0.0096 = 2269.5 \text{ N/mm}^2$$

7. Checking force equilibrium to verify the initial assumption of the neutral axis ( $c$ ), where the parameters of  $\alpha_1, \beta_1, \varepsilon_c$  are calculated as shown in (6, 7, 8), respectively.

$$\varepsilon_c = \frac{1.7f_c'}{E_c} = \frac{1.7 \times 35.81}{28,430} = 0.0021 \text{ mm/mm}$$

$$\beta_1 = \frac{4\varepsilon_c' - \varepsilon_c}{6\varepsilon_c' - 2\varepsilon_c} = \frac{4 \times 0.0021 - 0.0023}{6 \times 0.0021 - 2 \times 0.0023} = 0.759$$

$$\alpha_1 = \frac{3\varepsilon_c' \varepsilon_c - \varepsilon_c^2}{3\beta_1 \varepsilon_c'} = \frac{3 \times 0.0021 \times 0.0023 - 0.0023^2}{3 \times 0.759 \times 0.0021} = 0.907$$

$$c = \frac{573 \times 345 + 44 \times 2269.5}{0.907 \times 35.81 \times 0.759 \times 200} = 60.39 \text{ mm} \neq 50 \text{ mm}$$

Revising the assumption of the neutral axis ( $c$ ), and repeating from steps 4 to 7 until the equilibrium is achieved.

8. Adjusting the depth to the neutral axis ( $c = 56.94$  mm) until the equilibrium is satisfied and the final results are  $\varepsilon_s = 0.0091$ ,  $\beta_1 = 0.786$ ,  $\alpha_1 = 0.928$

$$c = \frac{573 \times 345 + 44 \times 2269.5}{0.928 \times 35.81 \times 0.786 \times 200} = 56.94 \text{ mm}$$

9. Calculating the maximum moment based on (18).  
- The contribution of steel bars in the tension region:

$$M_s = 573 [345 + 2000(0.0091 - 0.0017)] (250 + 0.5 \times 0.786 \times 56.94)$$

$$\Rightarrow M_s = 46.92 \text{ kN} \cdot \text{m}$$

- The contribution of FRP bars:

$$M_f = 44 \times 2269.5 (286.5 - 0.5 \times 0.786 \times 56.94)$$

$$\Rightarrow M_f = 26.37 \text{ kN} \cdot \text{m}$$

- The contribution of steel bars in the compression region:

$$M_{s'} = 142.7 \times 345 (50 - 0.5 \times 0.786 \times 56.94)$$

$$\Rightarrow M_{s'} = 1.36 \text{ kN} \cdot \text{m}$$

- The maximum moment

$$M_n = 46.92 + 0.85 \times 26.37 - 1.36$$

$$\Rightarrow M_n = 67.98 \text{ kN} \cdot \text{m}$$

#### APPENDIX B. DESIGN FOR FRP NSM METHOD

Fig. 16 illustrates the dimension of FRP bar and material properties of concrete and steel are described in Table VII. The steps of design are presented as follows:

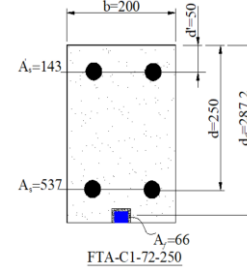


Figure. 16 Section of the NSM FRP bar. Unit: N, mm

1. Determining factored moment ( $M_u$ ) as shown in (21) with assumption  $M_{DL} = 29 \text{ kN} \cdot \text{m}$ , and the live moment ( $M_{LL}$ ) is assumed to be  $45 \text{ kN} \cdot \text{m}$

$$M_u = 1.1M_{DL} + 0.75M_{LL} = 1.1 \times 29 + 0.75 \times 45$$

$$\Rightarrow M_u = 65.65 \text{ kN} \cdot \text{m}$$

2. Determining the design values of FRP bar using the environmental reduction factor as shown in (3) with  $C_E = 0.95$  and preliminary calculating the area ( $A_f$ ) of externally bonded FRP bar is assumed to be  $0.333b$

$$f_{fu} = C_E f_{fu}^* = 0.95 \times 3990 = 3790.5 \text{ N/mm}^2$$

$$\varepsilon_{fu} = C_E \varepsilon_{fu}^* = 0.95 \times 0.0168 = 0.0159 \text{ mm/mm}$$

$$A_f = 0.333b = 0.333 \times 200 \approx 66 \text{ mm}^2$$

3. Calculating the initial strain level on bonded substrate ( $\varepsilon_{bi}$ ) by (13) with  $k = 0.329$ ;  $M_{DL} = 29 \text{ kN} \cdot \text{m}$  and  $I_{cr} = 175 \times 10^6 \text{ mm}^4$

$$\varepsilon_{bi} = \frac{M_{DL} (d_f - k.d)}{I_{cr} E_c} = \frac{29 \times 10^6 (287.2 - 0.329 \times 250)}{175 \times 10^6 \times 28,430}$$

$$\Rightarrow \varepsilon_{bi} = 0.0011 \text{ mm/mm}$$

4. Assuming and adjusting the depth to the neutral axis ( $c$ ) until the equilibrium is satisfied and the final results are:

$$c = 64.8 \text{ mm}, \beta_1 = 0.851, \varepsilon_s = 0.0096, f_{fe} = 2269.5 \text{ N/mm}^2$$

5. Calculating the ultimate flexural strength of the section by (18), where  $\phi = 0.9$

$$M_n = M_s + \omega M_f - M_{s'} = 45.98 + 0.85 \times 36.31 - 1.10$$

$$\Rightarrow \phi M_n = 0.9 \times 75.75 = 68.17 \text{ kN} \cdot \text{m} > M_u = 65.65 \text{ kN} \cdot \text{m}$$

The required design of the flexural strength exceed the factored moment.

6. Designing the details of FRP bar by (24).

The number of FRP (density and fineness show in Table I):

$$n' = \frac{A_f \times \rho}{g} = \frac{66 \times 1.8 \times 1000}{1650} = 72 \text{ strands}$$

(FTA-C1-72-205)

The dimensions of groove:

$$3a_f \times 3a_f = (25 \times 25) \text{mm}$$

$$(3a_f = 3\sqrt{66} \approx 25 \text{mm} \Rightarrow a_f = b_f = 8.3 \text{mm})$$

The developed length of FRP bar (the average bond strength ( $\tau_b$ ) is estimated about 6.9 MPa):

$$l_d = \frac{a_f \times b_f}{2(a_f + b_f)} f_{fe} = \frac{8.3 \times 8.3}{2(8.3 + 8.3)} 2269.5$$

$$\Rightarrow l_d \approx 685 \text{mm}$$

#### ACKNOWLEDGMENT

Akira Kobayashi (Development department, Nippon Steel & Sumikin Materials Co., Ltd. Composite Company), and Takafumi Yamaguchi, Kazuki Ohshita, Nguyen Thu Nga, who are students of Kanazawa University contributed to pursuit experiment. The author expresses great thanks to them. This study had been done by the support of Cross-ministerial Strategic Innovation Promotion Program (SIP).

#### REFERENCES

- [1] A. Naaman, S. Y. Park, M. Lopez et al., "Glued-on fiber reinforced plastic (FRP) sheets for repair and rehabilitation," The University of Michigan, Department of Civil and Environmental Engineering, MI 48109-2125, 1977.
- [2] A. H. Abdullah and M. R. A. Kadir, "NSM FRP reinforcement for strengthening reinforced concrete beams-overview," *ZANCO Journal of Pure and Applied Sciences*, vol. 28, pp. 178-200, 2016.
- [3] R. Parretti and A. Nanni, "Strengthening of RC members using near-surface mounted FRP composite: Design overview," *Journal of Advances in Structural Engineering*, vol. 7, no. 5, 2004.
- [4] W. Jung, J. Park et al., "Flexural behavior of concrete beam strengthened by near-surface mounted CFRP reinforcement using equivalent section model," *Journal of Hidawi, Advances in Materials Science and Engineering*, Article ID 9180624, 2017.
- [5] ACI 440.2R-08, "Guide for the design and construction of externally bonded FRP systems for strengthening concrete structures," American Concrete Institute, 2008.
- [6] ACI 440.1R-15, "Guide for the Design and construction of structural concrete reinforced with Fiber-Reinforced Polyme (FRP) bars," American Concrete Institute, 2015.
- [7] ACI 318-05, "Building code requirements for structural concrete," American Concrete Institute, 2005.
- [8] LS-DYNA "Keyword user's manual," Livermore Software Technology Corporation, 2016.
- [9] H. Jiang and J. Zhao, "Calibration of the continuous surface cap model for concrete," *Journal of Finite Elements in Analysis and Design*, vol. 97, pp 1-19, 2015.
- [10] H. Jiang, X. Wang et al., "Numerical simulation of Impact test on reinforced concrete beam," *Journal of Material and Design*, vol. 39, pp. 111-120, 2015.
- [11] K. Yoten, M. Manzari et al., "An assessment of constitutive models of concrete in the crash worthiness simulation of roadside safety structure," *International Journal of Crashworthiness*, vol. 10, pp. 5-19, 2005.
- [12] Demetrios M. Cotsovos, "A simplified approach for assessing the load-carrying capacity of reinforced concrete beams under concentrated load applied at high rates," *International Journal of Impact Engineering*, vol. 37, pp. 907-917, 2005.



**Trung Tran Le Hoang** is a Ph.D Candidate from Graduate school of Natural Science and Technology, Kanazawa University, Kakuma-machi, Kanazawa 920-1192, Japan. He was a Lecturer who worked for Dept. of Civil Engineering, Kien Giang College, 425 Mac Cuu, Vinh Thanh, Rach Gia, Kien Giang, Viet Nam. The current address is NST-2C330, Kakuma-machi, Kanazawa city, Ishikawa, Japan. He attained Bachelor degree of Civil Engineering from Faculty of Civil Engineering, Ho Chi Minh University of Architecture in 2005. And in 2012, he got Master of Engineering from Faculty of Civil Engineering, Ha Noi University of Architecture. In 2016, he was a Ph.D student in Graduate school of Natural Science and Technology, Kanazawa University, Japan.



**Hiroshi Masuya** works in the Faculty of Geosciences and Civil Engineering, Institute of Science and Engineering, Kanazawa University. The address is Kakuma-machi, Kanazawa 920-1192, Japan. He worked as Research assistant of Kanazawa University in 1982, and in 1989 received the Doctor degree of Engineering from Osaka City University. In 1992, he became the Assistant professor for Kanazawa University. During 1992-1993, he was Guest researcher of Swiss Federal Institute of Technology. In 1993 he became Associate professor of Kanazawa University, and Professor of Kanazawa University in 2003. He joined Academic Society & Scientific Organization such as Japan Society of Civil Engineers, Japan Concrete Institute, The Japan Society for Computational Engineering and Science



**Kubo Yoshimori** is from Faculty of Geosciences and Civil Engineering, Institute of Science and Engineering, Kanazawa University. The address is Kakuma-machi, Kanazawa 920-1192, Japan. In 2000, he received the Doctor degree from Kyoto University. He became the Professor of Kanazawa University. The Academic Society & Scientific Organization he joined is Japan Society of Civil Engineers



**Hiroshi Yokoyama** works for Research Institute for Infrastructure Engineering, Nippon Engineering Consultants Co., Ltd., Japan. The address is L. A. Tower 11-2 Shintoshin Chuo-ku Saitama 330-6011, Japan. In 2013, he received the Doctor degree of Engineering from Kanazawa University. He joined Academic Society & Scientific Organization as Japan Society of Civil Engineers